Coupling and Feedback in the Manna Universality Class

Dan Barker[1] and Haye Hinrichsen[2*]

[1] *Complexity Science, University of Warwick, Coventry, CV4 7AL, UK.*
[2] *Fakultät für Physik and Astronomie, Universität Würzburg, D-97074 Würzburg, Germany.*
[*] *supervisor*

Abstract

Understanding the link between various universality classes of non-equilibrium phase transitions is an important question and has direct consequences across many different disciplines. To that end we investigated properties of the conserved Manna sandpile model and attempted to construct a variant of the contact process which shared the Manna universality class behaviour. For the Manna model the relative excess of particles and density of active sites were found to scale with exponents $\alpha = 0.208(2)$ and $\delta = -0.176(3)$ with time and $\beta = 1$ and $\gamma = 0.333(7) \simeq 1/3$ with density respectively. A variant of the contact process was defined which coupled the activity to a conserved background field as in the Manna model and the properties measured. Similar scaling behaviour was not found for this model.

1 Introduction

Self-organised criticality is a topic which has attracted much attention in recent years [1–5]. It usually occurs in cases where the system is slowly driven and the driving force is dissipated quickly but sporadically, usually in some form of spontaneous energy cascade or avalanche. Such systems are diverse, ranging from earthquake models [6] to interface depinning [1]. Despite the fact the models are quite different they seem to display similar behaviour at criticality, this is called *universality* [7, 8]. Traditionally the most active area of focus for investigations into self-organised criticality has been sandpile models, starting with the BTW model in 1987 [9].

If the system is driven slowly with energy escaping from the boundaries the system approaches and then remains in a critical state where we see energy cascades of all sizes distributed as a power law [9]. Therefore this set up is known as the self-organised criticality (SOC) ensemble. If instead we impose periodic boundary conditions so that energy cannot escape and we no longer drive the system so the energy in the system remains constant we are then in the so called fixed-energy ensemble. In this case the system no longer approaches criticality by itself but can be made to exist at its critical point by tuning the amount of energy in the system. This is the control parameter. In this fashion we establish a link between self-organised and ordinary criticality. For sandpile models the 'energy' is the number of particles that sit on the lattice, so in the fixed-energy ensemble we have a conserved number of particles in the system and the control parameter is the density of particles.

By changing this control parameter one can observe an absorbing phase transition, i.e. a transition from a fluctuation into a frozen phase. Below the critical density the system can reach states where all activity has ceased. Above this critical density however the activity will carry on *ad infinitum* (in an infinite system).

In this project we examine a sandpile model called the conserved Manna model [10] which is the subject of much current research. The Manna model differs from deterministic models such as the BTW model in that it is a stochastic sandpile model. This inherent stochasticity is a desirable feature which leads to less artifacts which could obscure universal behaviour [11]. Like other models the Manna model exhibits an absorbing phase transition when in the fixed energy ensemble.

The work is motivated by a long-standing debate about the nature of the transition in this model. In particular a possible relation to the universality class of Directed Percolation (DP).

1.1 The Manna Model

In the Manna model particles sit on the sites i of a lattice Λ. The number of particles on a particular site i is $z_i \in \mathbb{Z}^+$. We divide the sites into two classes: inactive and active. If $z_i < 2$ the site i is inactive,

The Manna Model	
1.	Initialise temporary lattice: for all sites i set $z'_i(t) = z_i(t)$.
2a.	For all sites i if $z_i(t) \geq 2$ go to step 2b.
2b.	Set $z'_i(t) = z'_i(t) - z_i(t)$.
	Pick a new site $j = i \pm 1$ with probability 0.5, increment $z'_j(t) \to z'_j(t) + 1$.
	Repeat $z_i(t)$ times.
3.	Copy temporary lattice into actual lattice: for all sites i set $z_i(t+1) = z'_i(t)$.

Table 1: Algorithm for simulating the Manna model on a computer.

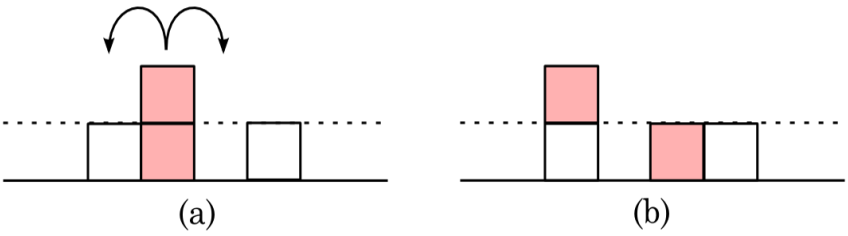

Figure 1: The update scheme for an active site in the Manna sand-pile model. In (a) the active site is updated leading to the configuration (b) in which a new site has become active. This is just one of three possible outcomes of the update rule for this configuration.

otherwise it is active. The update of the lattice only affects *active* sites, which it does by redistributing all of the particles on the active site to its nearest neighbours with equal probability for each particle. For example in 1-d updating an active site with $z_i = 2$ leads to both particles being shifted to either $i-1$ or $i+1$ with probability 0.25 and one to both $i+1$ and $i-1$ with probability 0.5. It is this inherent stochasticity in the update rule that leads to the Manna model being called a stochastic sandpile model. All active sites are updated in parallel with the algorithm shown in Table 1. Naturally this update can lead to previously inactive sites becoming active as shown schematically in Figure 1

In this investigation we restrict ourselves to one spacial dimension and time, the (1+1)-d case and impose periodic boundary conditions on the lattice Λ. Thus we are working in the *fixed-energy ensemble* instead of the self-organised criticality (SOC) ensemble which has attracted much attention previously . It is conjectured that Directed Percolation models and the Manna model belong to distinct universality classes [12, 13]: the DP and Manna or C-DP respectively. This is supported by numerical evidence [14–16]. The Langevin equation for the DP universality class is

$$\frac{\partial \rho}{\partial t} = -r\rho - b\rho^2 + \nabla^2 \rho + \sigma\sqrt{\rho} \cdot \eta(\mathbf{x}, t). \tag{1}$$

Where $\rho = \rho(\mathbf{x}, t)$ is the activity density and $\eta(\mathbf{x}, t)$ is a noise term. In the Manna model we must consider two fields: the density of particles and the density of active sites. According to conjecture by Muñoz et al [17] this leads to a slight modification of the DP Langevin equation yielding the coupled stochastic partial differential equations

$$\frac{\partial \rho}{\partial t} = -r\rho - b\rho^2 + \nabla^2 \rho + \sigma\sqrt{\rho} \cdot \eta(\mathbf{x}, t) + \omega\rho \cdot \phi, \tag{2}$$

$$\frac{\partial \phi}{\partial t} = D\nabla^2 \rho. \tag{3}$$

Where $\rho = \rho(\mathbf{x}, t)$ is again the density of *active sites*, $\eta(\mathbf{x}, t)$ is a white noise term and $\phi = \phi(\mathbf{x}, t)$ is the density of particles. Equation (1) is modified by a linear coupling of the active site density ρ to the particle density ϕ to become equation (2). This coupling captures the fact sites only become active in the discrete case when $z_i \geq 2$ and equation (3) encapsulates the fact that particles can only move by being redistributed from an active site.

1.2 Interface Models

It is possible to map sandpile models to models of interfaces moving through random quenched media and indeed much work on sandpiles also considers these interface models. Understanding such systems is important since it has applications in many areas of technology. One particular example is that of a magnetic domain wall moving through a material, a system clearly of importance for storage technologies.

In these models each point on the lattice has a height $H_x(t)$ which represents the penetration of an interface through a medium. The interface is pulled with some force F. The phase transition seen in the fixed-energy ensemble sandpiles manifests itself as a 'depinning transition' in the interface models. A depinning transition occurs at a critical pulling force F_c, at which point the interface becomes unstuck and is able to move through the medium. In the magnetic domain example mentioned previously the role of F is played by an external magnetic field. The dynamics of such 'linear interface models' (LIM) are governed by the quenched Edwards-Wilkinson (qEW) equation

$$\frac{\partial H}{\partial t} = \nabla^2 H + F + \eta(\mathbf{x}, t), \tag{4}$$

where $\eta(\mathbf{x}, t)$ is a white noise. The height of the interface $H = H(\mathbf{x}, t)$ can be mapped to the sandpile as counting how many times a particular site has toppled, that is

$$H(x, t) = \int_0^t \rho(x, s) ds. \tag{5}$$

The exact nature of the noise terms in the mapped interface model depend on the sandpile model considered. For instance the BTW and Manna models have different noise terms in (4). For a fuller discussion of the mapping see [18], [19] and [1].

The existence of such mappings means that any progress in understanding sandpiles has direct implications for the comprehension of these interface models. Indeed recent work by Bonachela et al [3] suggests that contrary to previous numerical studies [4] the Manna and LIM universality classes are equivalent.

2 Observables

In the Manna model particles are not evenly spread along the lattice. If they were the system would be in an absorbing state (unless $\bar{\phi} > 1$). So a natural question to ask it how are the particles distributed on the lattice? One measure we can use to quantify this is the excess or deficit of particles to the left of a point relative to the average density. Mathematically we write this as

$$S(x, t) = \int_0^x \phi(y, t) dy - x\bar{\phi}, \tag{6}$$

where

$$\bar{\phi} = \frac{1}{L} \int_0^L \phi(y, t) dy. \tag{7}$$

Equations (6) and (7) are general for continuous systems. However our model in fact lives on a discrete 1-d lattice of length L. For this case we can write $\bar{\phi} = \frac{N}{L}$ where N is the number of particles. $S(x, t)$ becomes

$$S_x(t) = \left(\sum_{i=1}^{x} z_i(t) \right) - \frac{xN}{L}. \tag{8}$$

Note that the number of particles on site x, $z_x(t)$ directly represents $\phi(x, t)$. Of particular note is the behaviour of the variance of $S_x(t)$.

Care must be taken if we wish to compare the distribution of $S_x(t)$ from many different realisations. The reason for this is that the values of $S_x(t)$ clearly depend on which lattice site we define to be 'zero'. Since we are using periodic boundary conditions the choice is completely arbitrary but this choice can affect the values of S_x, as illustrated in Figure 2. The two density profiles shown (ϕ and ϕ') are equivalent under periodic boundary conditions but by arbitrarily defining a zero point we have affected S_x. Since

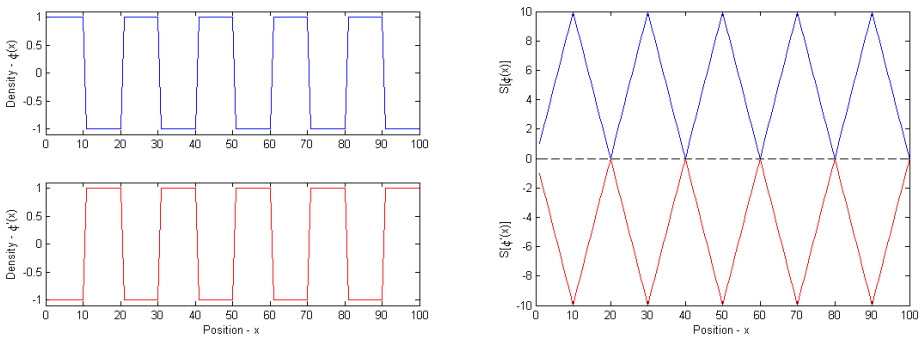

Figure 2: Because equation 6 defines a zero point, two systems which are equivalent under periodic boundary conditions (*left*) can lead to different values of $S_x(t)$ (*right*) so care must be taken when combining measurements from various realisations.

The Contact Process	
1.	Pick a random site i.
2a.	If $s_i(t) = 1$ then set $s_i(t+1)$ to zero with probability $1/(1+\lambda)$.
2b.	Else count the number of neighbours that have value 1, call this n. Set $s_i(t+1)$ to one with probability $n\lambda/(2(1+\lambda))$.
3.	Increment time by $\Delta t = 1/L(1+\lambda)$.

Table 2: Algorithm for simulating the contact process on a computer.

this choice will not affect the variance of S *for an individual realisation* we can average the measurements of VAR(S_x) as usual. However if we wish to look at the distribution of the S across many realisations we must take care to subtract the mean of S for each realisation before combining the values.

Another important observable is the average density of active sites $\bar{\rho}$. We can write this in a similar form to $\bar{\phi}$,

$$\bar{\rho}(t) = \frac{1}{L}\int_0^L \rho(y,t)dy. \tag{9}$$

In our discrete system this integral just equates to counting the number of active sites $N_A(t)$ so again we have a nice simple form $\bar{\rho}(t) = \frac{N_A(t)}{L}$.

3 Moving from Directed Percolation to Manna

According to the literature the Manna model belongs to a different universality class to Directed Percolation (DP) models such as the Domany-Kinsel automaton [20, 21]. A natural question to ask is then, what are the salient differences between models in the two classes and is it possible to move DP models into the Manna universality class?

The Manna Langevin equations (2) and (3) encode the coupling between the density of particles ϕ and the active sites ρ. In DP no such coupling exists, however we can try to artificially impose it. For a concrete example let us consider the contact process.

The contact process is a continuous time model where the sites on a lattice take the values either 1 or 0. If a site i has value $s_i(t) = 1$ it is set to 0 with rate $\omega(1 \to 0) = 1$, otherwise the site is set to 1 with rate $\omega(0 \to 1) = (n\lambda)/(2d)$ where n is the number of neighbouring sites which have value 1. We restrict d the spacial dimension to 1 because in that case we expect the differences between the DP and Manna classes to be most pronounced.

The control parameter for this model is λ. There is a critical value λ_c above which the process survives *ad infinitum* and below (and at) which the process will eventually die out and reach the unique absorbing state of all zeros. Like the phase transition shown by the Manna model this is an absorbing phase transition. Since this is a continuous time model we can simulate it using random sequential updates, specifically using the algorithm in Table 2.

Now we have defined the model we can try and impose a coupling similar to that in equations (2) and (3) by introducing a modified control parameter $\lambda \to \lambda + \varepsilon\phi$. In the standard contact process we have only ρ but from (3) we can write

$$\phi(x,t) = D\int_0^t \nabla^2\rho(x,s)ds. \tag{10}$$

We can approximate $\nabla^2\rho$ for our discrete model by using the discrete Laplacian

$$\nabla^2\rho \simeq \rho(x-1,t) - 2\rho(x,t) + \rho(x+1,t),$$

which provides a way to calculate ϕ for the contact process. We can also calculate the same quantities such as $S(x,t)$. By substituting equation (10) into (6) we get

$$S(x,t) = D\int_0^x\int_0^t \nabla^2\rho(y,s)ds\ dy - x\bar{\phi}. \tag{11}$$

In the contact process we do not have particles in the same sense as the Manna model. Thus we can no longer write $\bar{\phi} = \frac{N}{L}$ but instead we can calculate this quantity by using equation (7). Combining all of these gives

$$S(x,t) = D\int_0^x\int_0^t \nabla^2\rho(y,s)ds\ dy - \frac{xD}{L}\int_0^L\int_0^t \nabla^2\rho(y,s)ds\ dy, \tag{12}$$

which when converted to the discrete case becomes

$$\begin{aligned} S_x(t) \simeq & D\left(\sum_{y=1}^{x}\sum_{s=1}^{t}\rho_{y-1}(s) - 2\rho_y(s) + \rho_{y+1}(s)\right) \\ & - \frac{xD}{L}\left(\sum_{y=1}^{L}\sum_{s=1}^{t}\rho_{y-1}(s) - 2\rho_y(s) + \rho_{y+1}(s)\right). \end{aligned} \tag{13}$$

Since we are working with periodic boundary conditions we can identify $\rho_0(t) = \rho_L(t)$ and $\rho_{L+1}(t) = \rho_1(t)$ which means the second term in (13) is identically zero. Additionally in the Manna model $D = d^{-1}$ [18] so here where $d = 1$ this disappears from the equations and we are left with the simplified estimate

$$S_x(t) \simeq \sum_{y=1}^{x}\sum_{s=1}^{t}\rho_{y-1}(s) - 2\rho_y(s) + \rho_{y+1}(s). \tag{14}$$

The fact that the second term in (13) is identically zero for all times is important since it means that our constructed ϕ_x is a conserved field as it is in the fixed-energy ensemble Manna model. Writing S_x in this form opens another interpretation as to what it represents. The discrete Laplacian at site x is equal to the current flow of particles at x, see (3). By integrating this over time we are measuring the balance of inflow and outflow of particles to and from site x. Thus we can also interpret S_x to be the balance of flow from the left of x to the right against flow to the right of x to the left.

Universality classes are defined by the behaviour of their models at criticality thus if this coupling does move the model from the DP to the Manna universality class we would expect to see the same scaling behaviour as for the Manna model.

4 Results

4.1 Scaling

We began by simulating the Manna model at the critical density of $\bar{\phi}_c = 0.8924$ and observing the scaling properties of the variance of the particle density fluctuations, $\mathrm{VAR}(S) = \sigma_S^2$ and density of active sites ρ. These quantities are expected to scale with power law behaviour, i.e.

$$\begin{aligned} \sigma_S^2 \sim t^\alpha, \quad \sigma_S^2 \sim \Delta\phi^\beta, \\ \rho \sim t^\delta, \quad \rho \sim \Delta\phi^\gamma, \end{aligned}$$

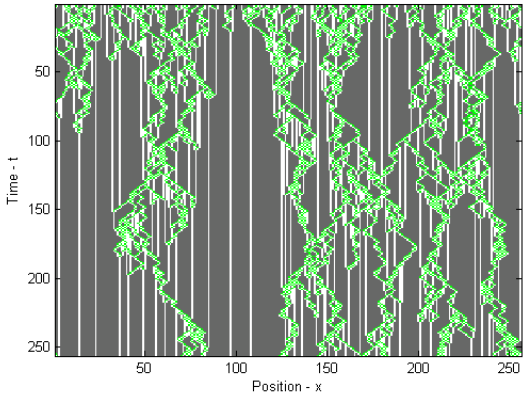

Figure 3: An example run of the Manna model in the super-critical phase with $\bar{\phi} = 0.9$. Empty sites are shown in white, sites with a single particle in grey and active sites in green. Note that active sites may have more than two particles.

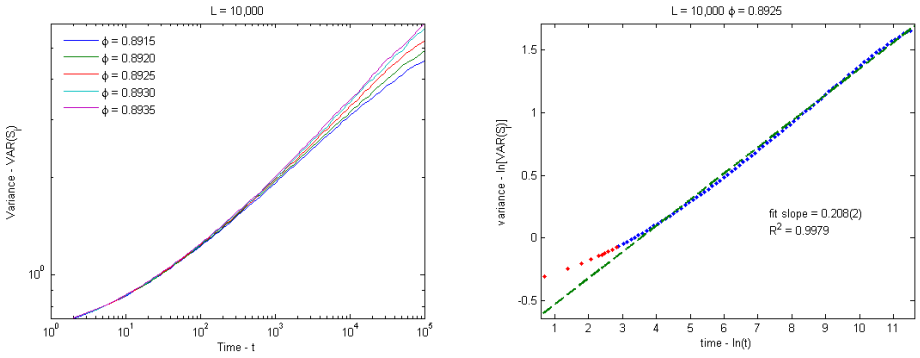

Figure 4: (*left*) The variance of S against time for several densities averaged over 1000 realisations. We can see that only at the critical density does it obey a power law. (*right*) Fitting a power law yields an exponent of $\alpha = 0.208(2)$.

where t is the time and $\Delta\phi = |\bar{\phi}_c - \bar{\phi}|$ is the distance from criticality.

For simulations of this kind the initial conditions are of importance [14]. To set up the initial conditions two steps were followed. Firstly the system was set up into a regular absorbing state, i.e. all particles distributed evenly so that no sites are active. Then a *short* diffusion is allowed to take place whereby on average each particle is allowed to jump to one of its neighbouring sites, activating the system. Such initial conditions are called 'natural initial conditions'.

Natural initial conditions are used because they reduce transitory behaviour and give cleaner results for the scaling exponents. Since we are close to an absorbing state the correlations which exist in the natural initial conditions are more representative of the real system than distributing the particles randomly [22]. An example system above criticality is shown in Figure 3.

It is clear from Figure 4 that the variance σ_S^2 obeys a power law increasing in time with exponent $\alpha = 0.208(2)$. In addition we observed that σ_S^2 scales *linearly* with the distance above the critical point $\Delta\phi$. This is somewhat surprising as it means the scaling exponent β in this case is unity.

The scaling properties of the density of active sites $\bar{\rho} = N_A/L$ was also measured. For scaling with time we find a scaling exponent of $\delta = -0.176(3)$ and for scaling with $\Delta\phi$ we find an exponent of $\gamma = 0.333(7) \simeq 1/3$. The fits for these are shown in Figure 6.

4.2 Finite Size Scaling

Next the behaviour under scaling of the system size at criticality was measured. System sizes ranging from $L = 16 = 2^4$ to $L = 16384 = 2^{14}$ were simulated. Given this data it is possible to make use of the

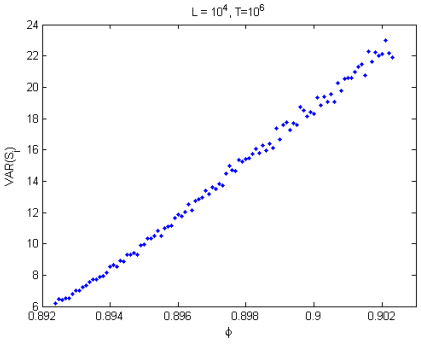

Figure 5: The variance of S against the distance from criticality averaged over 1000 realisations. We can see that the scaling is linear which implies $\beta = 1$.

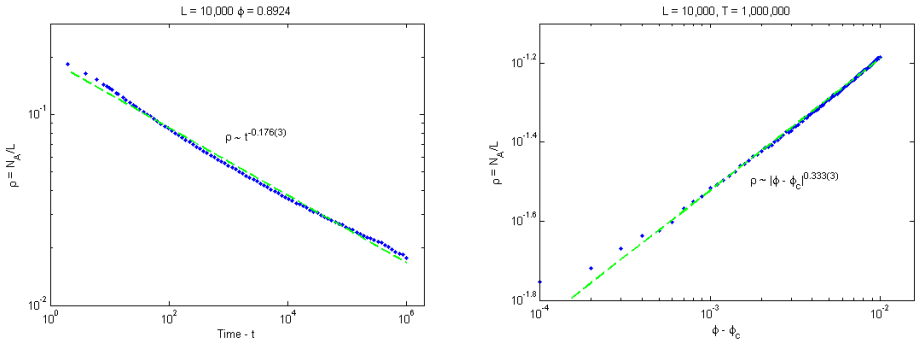

Figure 6: (*left*) The average density of active sites versus time scales with exponent $\delta = -0.176(3)$. (*right*) The average density of active sites versus the distance from criticality scales with exponent 0.333(7). Both plots were averaged over 10^3 realisations.

finite size scaling ansatz. This states that there exists a so called 'scaling function' whose behaviour is independent of L but not of the critical exponents. Mathematically we write the ansatz as

$$\rho = L^{\nu}\tilde{\rho}(L^{-z}t), \tag{15}$$

where $\tilde{\rho}(\cdot)$ is the scaling function. This means that if $\rho L^{-\nu}$ is plotted against $L^{-z}t$ we will see the data from all system sizes collapse onto one curve, if and only if we choose the correct critical exponents ν and z.

It was found that data collapse occurred for the density of active sites ρ when the following rescaling was used: $\rho/L^{-0.32}$ versus $t/L^{1.64}$. For the variance of particle excess σ_S^2 we found that rescaling $\sigma_S^2/L^{0.43}$ versus $t/L^{1.95}$ causes the peaks to collapse. These collapses are shown in Figure 7.

Additionally if we examine the saturation variance $\sigma_S^2(\infty)$ as a function of system size L we find a clear power law $\sigma_S^2(\infty) \sim L^{0.60(1)}$ as shown in Figure 8. Naturally by changing the scaling exponent for σ_S^2 to 0.60 we obtain the data collapse with coincident saturation variances (not shown), that is a scaling of $\sigma_S^2/L^{0.60}$ versus $t/L^{1.95}$.

4.3 Density Fluctuations

The next quantity which was examined was the distribution of the excess of particles compared to its mean S_x. Figure 9 shows the distribution of S_x at criticality for a lattice size of $L = 16384$. Fitting a Gaussian curve to this distribution results in a reasonable fit but there is clear discrepancy at the peak and in the mid tails. A much better fit can be obtained by fitting a distribution of the form

$$f(x) \propto \exp\left[-\left(\frac{|x-\mu|}{\sigma}\right)^{d}\right]. \tag{16}$$

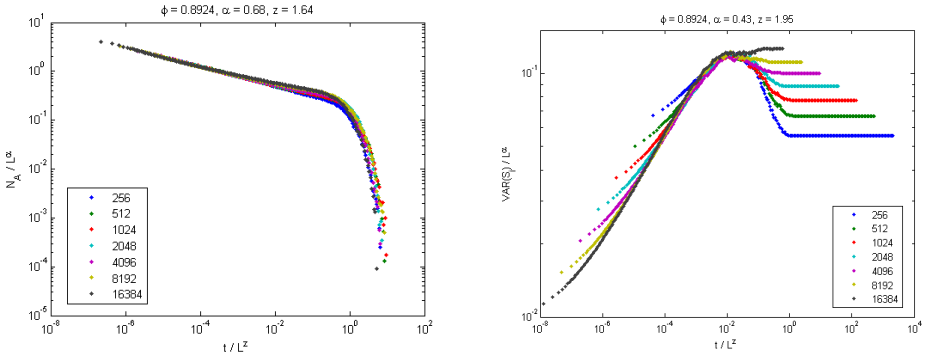

Figure 7: (*left*) Data collapse of the density of active sites against time. We can see that the scaling of $\rho/L^{-0.32}$ and $t/L^{1.64}$ leads to a good collapse. (*right*) With the variance of S we can either collapse the peaks of the curves or the saturation variance. Scaling as $\sigma_S^2/L^{0.43}$ versus $t/L^{1.95}$ yields a collapse where the peaks coincide nicely.

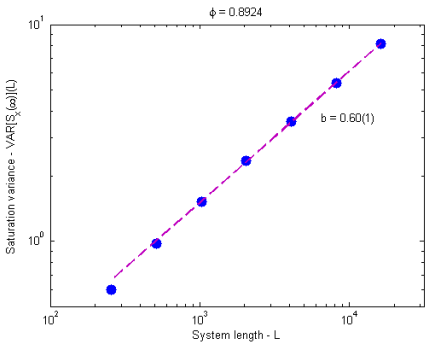

Figure 8: The saturation variance, when plotted against system size, follows a power law with exponent 0.60(1).

This equation is a trivial extension of the stretched exponential distribution [23] from $[0, \infty)$ to the whole real line. Unfortunately for such a distribution the normalisation constant and CDF must be computed numerically or using a series expansion. Despite this limitation the stretched exponential can take on large range of shapes which make it quite versatile. It can be seen by simple rearrangement of equation (16) that

$$\ln[-\ln[f(x)]] \propto d \ln|x - \mu|. \tag{17}$$

Using this equation if we plot $\ln[-\ln[f(x)]]$ against $\ln|x - \mu|$ the data should form a straight line with gradient d. Indeed this is what we see in Figure 9 with $d = 1.67(1)$. Additionally we can fit equation (16) as it is to the raw data which yields a slightly different value of $d = 1.617(1)$. The data used to produce this distribution were taken from 1000 realisations with $L = 16384$ meaning in total there were some 16384000 measurements of S_x.

4.4 Measured Correlations

Next we measured the autocorrelation of both S_x and ϕ_x, they are shown in Figure 10. For S_x we can see that there are long range correlations spanning the whole system. In contrast ϕ_x the density of particles has much shorter range correlation of around 5 lattice sites. The autocorrelation of ϕ_x is initially negative and then returns to zero. This is consistent with what one would expect based on the nature of the Manna model and the Langevin equation (3).

The negative correlation indicates that if there are particles located at x then there are likely to be less on the surrounding lattice sites, and conversely if x is empty then there are likely to be particles close by. This is because the particles can only move from active sites so if a site has particles it has received them from a previously active site. According to the redistribution rules (see Table 1) updating

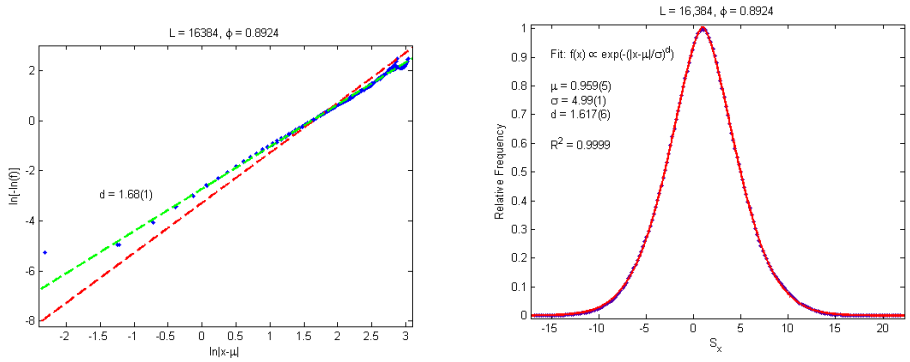

Figure 9: (*left*) Plotting $\ln[-\ln(f)]$ against $\ln|x-\mu|$ allows us to see that the fluctuations are not entirely Gaussian. If this were a Normal distribution the gradient of the slope would be identically 2 (shown in red) and instead here it is 1.68(1) (shown in green). (*right*) Fitting an equation of the form $f(x) \propto \exp(-(|x-\mu|/\sigma)^d)$ with μ,σ and d as free parameters yields a value of $d = 1.617(1)$. Note the two values should coincide which is not the case, suggesting that the values for d should be taken with considerations. However both show that there is some non-Gaussianity.

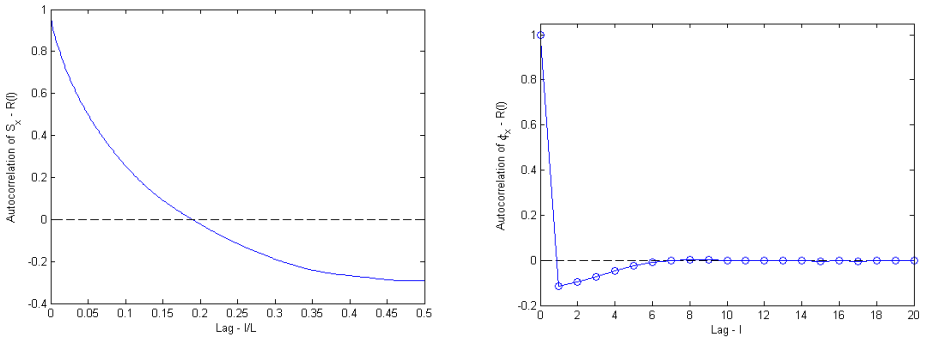

Figure 10: (*left*) The autocorrelation of S_x against the lag as a fraction of the system size, averaged over 1000 realisations. We can see it exhibits long range correlations. (*right*) The autocorrelation of ϕ_x averaged over 1000 realisations. Initially the correlation is negative before returning to zero after ~ 5 lattice sites.

an active site removes all the particles from this site so the number of particles will likely be less than surrounding sites to which it loses its particles, and by reciprocity if x is empty then the surrounding sites will have more particles since they have just been redistributed from x.

4.5 The Effect of Correlations

The Manna model has non-trivial, albeit short range, correlations in ϕ. To find a simpler example and observe the effect of strong correlations on the fluctuations S we used the method described in §3 and applied it to a process which displays very strong correlations in both space and time: the Sierpiński gasket.

The implementation of this was a cellular automaton with an exclusive-or (XOR) update rule, i.e. $000 \to 0$, $100 \to 1$, $001 \to 1$, $101 \to 0$. With this update rule we have to be careful about choosing the system size. It is not uncommon to use a system size which is a power of two, indeed for most of this investigation a system size of $L = 16384 = 2^{14}$ has been used. However, in this specific case this causes problems since the process rapidly annihilates itself if $L = 2^n$. This is illustrated in Figure 11. To combat this a system size of $L = 16382$ was used instead.

When the XOR process is run for 5×10^4 iterations and averaged over 500 realisations the distribution of our calculated fluctuations S is *highly* non-Gaussian. Fitting a function of the form of equation (16) leads to a value of $d = 4.92(5)$ and $\sigma = 1326(2)$, see Figure 11. This lends support to the idea that spatio-temporal correlations lead to non-Gaussianity in the distribution of S.

While the Sierpiński gasket XOR process provides a nice illustration of the effect of correlations on

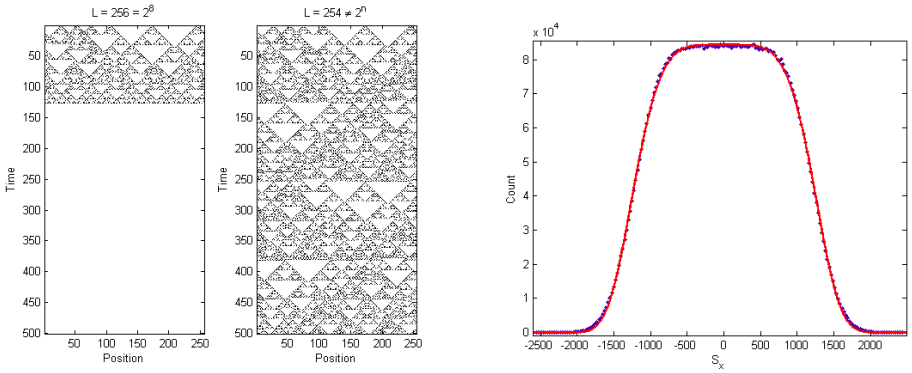

Figure 11: (*left*) The XOR process simulated with the same initial conditions with two different system sizes, $L = 256$ and $L = 254$. In the former case the process rapidly ceases while in the latter it continues ad-infinitum. The Sierpiński gasket like structure is also clearly visable. (*right*) Estimating the 'excess of particles' S for the XOR process leads to a highly non-Gaussian distribution with $d = 4.92(5)$.

S_x it is clearly unrealistic when compared to our system. Attempts were made to generate sequences of numbers with different autocorrelation functions. By making use of some basic properties of Fourier transforms it is possible to create sequences of numbers which have theoretically any arbitrary autocorrelation. The autocorrelation of a series is given by

$$R(\tau) = \langle f(t)f(t+\tau)\rangle = \int_{-\infty}^{+\infty} f(t)f(t+\tau)\,dt = f(t) * f(t), \tag{18}$$

where $*$ denotes convolution. By the Convolution Theorem a multiplication in Fourier space is equal to a convolution in real space so if we write $\tilde{f}(\omega) = \mathrm{FT}[f(t)]$ we obtain

$$\begin{aligned} R(\tau) &= \mathrm{FT}^{-1}[\tilde{f}(\omega)\cdot\tilde{f}(\omega)], \\ \Rightarrow \mathrm{FT}[R(\tau)] &= \tilde{f}(\omega)\cdot\tilde{f}(\omega), \\ \Rightarrow \tilde{f}(\omega) &= \mathrm{FT}[R(\tau)]^{1/2}. \end{aligned} \tag{19}$$

Using equation (19) we can write the power spectrum

$$S(\omega) = \tilde{f}(\omega)\cdot\tilde{f}^*(\omega) = (\mathrm{FT}[R(\tau)]^{1/2})\cdot(\mathrm{FT}[R(\tau)]^{1/2})^*. \tag{20}$$

Now we have the power spectral density $S(\omega)$ in terms of the autocorrelation $R(\tau)$, we can use this to generate a series which has any desired autocorrelation. In order to turn $S(\omega)$ into a series $f(t)$ we simply use the equation

$$f(t) = \int_{-\infty}^{+\infty} S(\omega)\sin[\omega t + \phi(\omega)]\,d\omega. \tag{21}$$

On its own $S(\omega)$ is not enough to reconstruct a signal since it contains no information about the phase of the signal but this is no issue here. By choosing $\phi(\omega) \sim U[0, 2\pi)$ we obtain what we desire: a sequence of seemingly random numbers that have the appropriate autocorrelation.

Equations (20) and (21) can be trivially converted to the discrete case. Attempts to utilise this method to generate signals suffered from the inherent limitation of finite sampling range. However the results (not shown) did display qualitative differences between signals with no correlation and signals exhibiting long range spatial correlations.

4.6 Coupling to a Conserved Field

As detailed in §1.1 the conjectured Langevin equations (2) and (3) couple the two fields ϕ and ρ together. Therefore we considered them separately in our simulation of the contact process and by applying the coupling detailed in §3 attempted to emulate the coupling present in the Manna model.

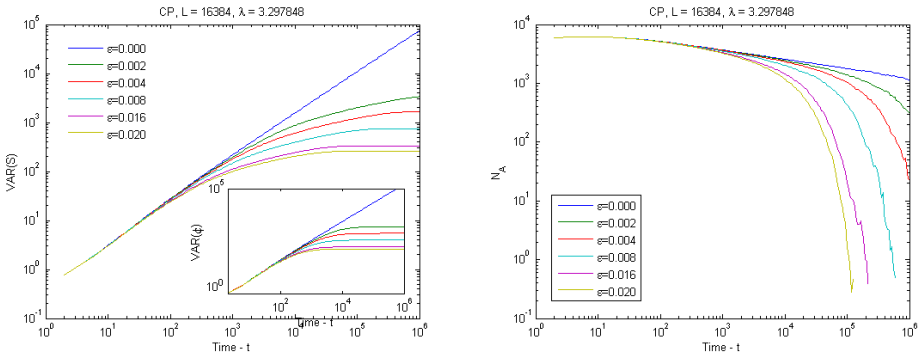

Figure 12: (*left*) The variance of our estimate for S against time for various coupling strengths (inset) The variance of particle density ϕ vs time for the same coupling strengths. (*right*) The number of active sites as a function of time for various coupling strengths ranging from 0 to 0.02.

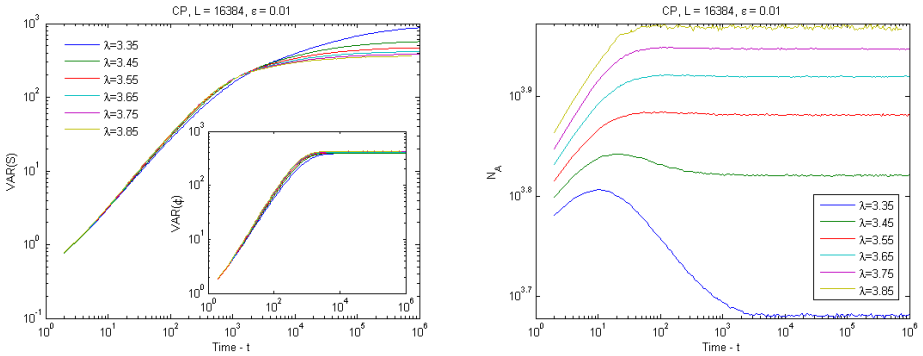

Figure 13: (*left*) The variance of S against time plotted for a range of λs (inset) the variance of calculated particle density ϕ for the same times and range of λ. (*right*) The number of active sites N_A as a function of time for a various values of λ.

We measured the behaviour of the usual quantities VAR(S) and ρ. For all coupling strengths ε examined VAR(S) initially follows a clear power law however with the coupling switched on it soon saturates and reaches a steady value. The reason for this is clearly seen if we instead look at the number of active sites N_A in Figure 12. We find that for higher ε the activity dies away sooner. Since S_x is effectively an integration over time of the discrete Laplacian at site x if the activity ceases then S_x will remain unchanging. The fact that increasing coupling strength ceases the activity sooner implies that it shifts the critical point so that we are now below criticality.

For zero coupling we do not observe a cessation of activity during the course of these simulations since we are at criticality. This however does not mean that it will not occur. Theoretically exactly at the critical point λ_c activity will eventually cease [24]. Unfortunately the computation times required for these simulations simply prohibited running them for longer.

This indication that by introducing the coupling we have shifted the critical point prompted us to fix $\varepsilon = 0.01$ and instead vary λ to try and find the new critical point $\lambda_c(\varepsilon)$. λ was varied from $\lambda = 3.25$ which is just below the original critical point to $\lambda = 3.95$ which is well above. The results are shown in Figure 13. The value of λ has a pronounced affect on the number of active sites N_A. As one would expect increasing λ leads to more sites being active. For all of the values of λ shown here the activity continues. After some initial transitory behaviour the activity settles a constant level. The saturation activity level $N_A(\infty)$ follows a power law against λ with exponent 0.24(1) and λ offset of 3.314(7), that is

$$N_A \sim |\lambda - 3.314(7)|^{0.24(1)}. \tag{22}$$

The behaviour of VAR(ϕ) seems to be largely unaffected by varying ε and for all values of λ simulated for VAR(S) we saw a departure from power law scaling.

5 Discussion

5.1 Correlations and Non-Gaussian Fluctuations

Let begin us by considering the completely uncorrelated case and what the distribution of S is. By completely uncorrelated we mean that $\phi(x) \sim \eta(x)$ where $\eta(x)$ is a white noise. Thus

$$S(x) = \int_0^x \eta(y)\, dy = B_x, \tag{23}$$

since the integral of white noise is a Brownian motion. For a Brownian motion B_x we know $B_x \sim N(0, x)$ with $N(0, \sigma^2)$ indicating a normal distribution with mean 0 and variance of σ^2. Thus we have for each x that $S(x) \sim N(0, x)$. Therefore naïvely disregarding correlations within sample paths the distribution of S across all sites x is the sum of many normal distributions. It is important to note that the *distribution* of S being a sum of Gaussian PDFs is different to S itself being the sum of many normally distributed random variables.[1] So we write

$$S \sim \sum_{x=1}^{L} N(0, x), \tag{24}$$

which in terms of the PDF is

$$f(S) = \frac{1}{L\sqrt{2\pi}} \sum_{x=1}^{L} \frac{1}{x} \exp\left(-\frac{S^2}{2x}\right). \tag{25}$$

The factor $1/L$ ensures $f(S)$ is normalised. This formula does not generalise so easily to the continuous case.

The distribution (25) shows perfect agreement with the numerical results of S calculated by taking ϕ to be a sequence of iid random variables $\sim N(0, 1)$. The resulting curve is highly non-Gaussian which can be seen intuitively by noticing that by adding many Gaussian PDFs with linearly increasing variance we are adding more and more to the tails of the distribution.

We neglected subtracting the mean of $S_x(\omega)$ for each sample path ω in the preceding discussion. Including this makes things much more complicated analytically but it should be considered since from simulations it appears to significantly affect the shape of the resulting distribution. However the previous serves to show that it is possible that at least some of the non-Gaussianity is a consequence of the structure of S_x itself. While this provides a nice illustration it is not the whole story, our results for the XOR process show that by giving ϕ strong spacio-temporal correlations the distribution of S becomes significantly more non-Gaussian than the case where ϕ is simply white noise.

Our measurements of the autocorrelation of ϕ (Figure 10) shows that the correlations in ϕ do exist but that they are relatively short lived. The previous means, unfortunately, that if these short range correlations do have some effect on the excess of particles it would be extremely difficult to detect with numerical simulations.

It is worth noting that while these inherent correlations in S make it difficult to consider the distribution of S across multiple realisations they are really the reason for using S instead of looking at ϕ itself. Examining ϕ_x only tells us about the site x, it provides no information about the density of particles around x. Measures such as S are capable of indicating whether the particles are spread evenly across the lattice, bunched together or something in between.

5.2 Universality Classes, Coupling and Feedback

The Manna and Directed Percolation (DP) universality classes, while distinct classes, clearly have similarities. As evidenced by the similarity of the Langevin equations and the apparent coincidence of the critical exponents [19]. Therefore it seems natural that by introducing a coupling of the form detailed in §3 one might to be able to take a DP model such as the contact process and move it into the Manna universality class.

The extensive numerical simulations run throughout the course of this project show that introducing this coupling has a significant impact on the behaviour of the activity within the contact process. Initial

[1] In fact each realisation S_x is a sum of many normally distributed random variables, which is why each S_x is itself normally distributed.

simulations with varying coupling strength ε showed that increasing ε while keeping the control parameter λ at the uncoupled critical value $\lambda_c = 3.297848$ caused the system's activity to die out sooner. This can be seen in the departure from power law behaviour for the variances of both S and ϕ and more explicitly in the behaviour of the number of active sites N_A, which drops to zero earlier and earlier for higher ε. The fact that the activity does drop to zero clearly implies that we are now in the sub-critical regime. Thus it appears the coupling has shifted the critical point away from the uncoupled value.

We sought to locate the new critical point by increasing λ and examining the behaviour of σ_S^2 and σ_ϕ^2 while keeping ε fixed at 0.01. As one would expect increasing λ causes the process to reach a stationary state with a higher level of activity. The final number of active sites follows a power law

$$N_A \sim |\lambda - \lambda_0|^\kappa, \tag{26}$$

where $\lambda_0 = 3.314(7)$ and $\kappa = 0.24(1)$. According to this power law the stationary activity level becomes zero at $\lambda = 3.314$ indicating the location of the critical point. Note however that the λ_0 is very close to the previous value of λ_c and forcing $\lambda_0 = \lambda_c$ gives only a slightly worse fit in terms of the value of R^2, being 0.9998 and 0.9977 respectively. Simulations run close to 3.314 indicate that the phase transition lies in the interval $\lambda_c \in (3.07848, 3.12848)$ for $\varepsilon = 0.01$. Unfortunately the length of time the simulations take to run prevented a more precise location of the critical point within the course of this investigation. For the smallest supercritical value of λ simulated the power law scaling of VAR(S) and $\bar{\rho}$ is not clear enough to determine in which universality class the model lies.

There are several conspicuous differences between the Manna model and the Contact Process which at first sight might appear to render them too different for the coupling to work. The two most conspicuous being discrete time versus continuous, and uniqueness of the absorbing state.

The Manna model is a discrete time process whereas the Contact Process is continuous time. This however is a property of the *model* and says nothing about the universality class. There exist discrete time models which are in the DP universality class, such as the Domany-Kinsel automaton. Plus one can easily envisage a continuous time version of the Manna model updated with random sequential updates rather than the parallel update of Table 1.

The Manna model has infinitely many absorbing states (for $L = \infty$) whereas the Contact Process has only one. Again there exist models in the DP class which have infinitely many absorbing states, for example the Pair Contact Process [20]. In addition this is a somewhat misleading interpretation. In the Manna model there are infinitely many states of ϕ which are absorbing. From the perspective of the activity ρ they are all the same, namely identically zero on the whole lattice. This is the same as in the contact process where the unique absorbing state is $\rho = 0$ for the whole lattice. In our coupled variant the estimated ϕ can also be in infinitely many states with $\rho = 0$ everywhere.

Thus we have reason to believe that these differences are not enough to affect which universality class our constructed model belongs to.

Additionally the effect of the coupling $\lambda \to \lambda + \varepsilon\phi_x$ should make the behaviour of ρ more similar to ρ in the Manna model. To see this consider the fact that ϕ_x is the time integral of the discrete Laplacian of ρ at site x. Thus if the site x is active and its neighbours are not then ϕ at the neighbouring sites will increase steadily increasing the probability that they become active. At the same time ϕ at x will be decreasing since ϕ is a conserved quantity which means that if site x becomes deactivated it will be less likely to be reactivated. In this fashion the coupling promotes the spreading of ρ but not its survival. This is much like ρ in the Manna model. When a site ρ is active it is updated so that it is no longer active and the particles distributed to its neighbours. This in turn makes the neighbouring sites more likely to be active and hence ρ spreads from a previously active site.

6 Conclusion

We first investigated the scaling properties of the conserved Manna model and found that the distribution of the corresponding interface variable S (see equation (8)) was mildly non-Gaussian. Examining a toy model in the shape of the XOR process shows that non-trivial correlations can have a large effect on the distribution of S. Unfortunately in the case of the Manna model it is hard to detect whether this non-Gaussianity is due to the spacio-temporal correlations which exist or the structure of S_x itself.

Next we constructed a variant of the contact process whereby the activity field ρ was coupled to a conserved background field ϕ and vice versa. The values of the conserved field ϕ depend on the values of

ρ up to the current time, clearly coupling ϕ to ρ. Then the control parameter was modified $\lambda \to \lambda + \varepsilon\phi$ thereby coupling ρ to ϕ analogously to the coupling present in the Manna model. It was then argued that apparent differences between the contact process and the Manna model should be superficial and would not affect the universal behaviour.

Despite introducing this coupling and arguing that it should cause ρ to behave like in the Manna model evidence that the new model had been moved to the Manna universality class was not found on the basis of the observables studied herein. Furthermore, solid evidence of criticality in the form of power law scaling of VAR(S) and $\bar{\rho}$ could not be identified. Examining the persistence of activity in the system as a function of λ places the critical point in the interval $\lambda_c \in (3.07848, 3.12848)$ for $\varepsilon = 0.01$. Further work is required to tighten these bounds and to determine if indeed the coupling is strong enough to have moved the system into the Manna class.

Acknowledgements

I would like to thank very much Prof. Haye Hinrichsen for supervising this project and providing logistical support, Dr. Stefan Großkinsky for helping to arrange my time in Germany, and everybody whom I met while here. Finally, this work was funded by the EPSRC.

References

[1] K.B. Lauritsen and M. Alava. Self-organised Criticality and Interface Depinning Transitions, 1999.

[2] M. Alava. Scaling in Self-organised Criticality from Interface Depinning. *J. Phys.: Condens. Matter*, 14:2353–2360, 2002.

[3] J.A. Bonachela, H. Chaté, I. Dornic, and M.A. Muñoz. Absorbing States and Elastic Interfaces in Random Media: Two Equivalent Descriptions of Self-organized Criticality. *Phys. Rev. Lett.*, 98(155702), Apr. 2007.

[4] J. Kockelkoren and H. Chaté. Absorbing Phase Transitions with Coupling to a Static Field and a Conservation Law, 2003.

[5] G. Pruessner and H.J. Jensen. Anisotropy and Universality: The Oslo Model, the Rice Pile Experiment and the Quenched Edwards-Wilkinson Equation. *Phys. Rev. Lett.*, 91(24), Dec. 2003.

[6] M. de Sousa Vieira. Self-organised criticality in a deterministic mechanical model. *Phys. Rev. A*, 46(10):6288–6293, 1992.

[7] J. Sethna. *Statistical Mechanics: Entropy, Order parameters and Complexity.* O.U.P., 2006.

[8] M. Paczuski and S. Boettcher. Universality in Sandpiles, Interface Depinning and Earthquake Models. *Phys. Rev. Lett.*, 77(1), July 1996.

[9] P. Bak, C. Tang, and K. Wiesenfeld. Self-organized Criticality: An Explanation of the 1/f Noise. *Phys. Rev. Lett.*, 59(4):381–384, Jul 1987.

[10] S.S. Manna. Large-scale simulation of avalanche cluster distribution in sand pile model. *J. Stat. Phys*, 59(1):509–521, 1990.

[11] R. Dickman, M. Alava, M.A. Muñoz, J. Peltola, A. Vespignani, and S. Zapperi. Critical Behavior of a One-dimensional Fixed Energy Stochastic Sandpile. *Phys. Rev. E*, 64(056104), Oct. 2001.

[12] W.G. Dantas and J.F. Stilck. Generalized Manna Sandpile Model With Height Restriction. *Braz. J. Phys.*, 36(3A):750–754, 2006.

[13] A. Hipke, S. Lübeck, and H. Hinrichsen. Absorbing Boudaries in the Conserved Manna Model. *J. Stat. Mech.*, 2009(07):P07021 (9pp), July 2009.

[14] M. Rossi, R. Pastor-Satorras, and A. Vespignani. Universality Class of Absorbing Phase Transitions with a Conserved Field. *Phys. Rev. Lett.*, 85(9):1803–1806, Aug. 2000.

[15] I. Dornic, H. Chaté, and M.A. Muñoz. Integration of Langevin Equations with Multiplicative Noise and the Viability of Field Theories for Absorbing Phase Transitions. *Phys. Rev. Lett.*, 94(100601), Mar. 2005.

[16] R. Pastor-Satorras and A. Vespignani. Reaction-diffusion System with Self-organized Critical Behavior. *Eur. Phys. J. B*, 19(4):583–587, 2001.

[17] A. Vespignani, R. Dickman, M.A. Muñoz, and S. Zapperi. Driving, Conservation and Absorbing States in Sandpiles. *Phys. Rev. Lett.*, 81(25):5676–5679, Dec. 1998.

[18] M. Alava and K. Bækgaard Lautritsen. Quenched Noise and Over-active Sites in Sandpile Dynamics. *Europhys. Lett.*, 53(5):563–569, Dec. 2000.

[19] M. Alava and M.A. Muñoz. Interface Depinning Versus Absorbing-state Phase Transition. *Phys. Rev. E*, 65(026145), Jan. 2002.

[20] M. Henkel, H. Hinrichsen, and S. Lübeck. *Non-Equilibrium Phase Transitions: Volume 1 Absorbing Phase Transitions*, volume 1 of *Theoretical and Mathematical Physics*. Springer, Dordrecht, The Netherlands, 2008.

[21] J.A. Bonachela and M.A. Muñoz. Confirming and Extending the Hypothesis of Universality in Sandpiles. *Phys. Rev. E*, 78(041102), 2008.

[22] P. Grassberger and A. de la Torre. *Ann. Phys. (N.Y.)*, 122(373), 1979.

[23] R. Kohlrausch. Theorie des Elektrischen Rückstandes in der Leidner Flasche. *Annalen der Physik und Chemie*, 91:56–82, 1854.

[24] C. Bezuidenhout and G. R. Grimmett. The Critical Contact Process Dies Out. *Ann. Probab.*, 18:1462–1482, 1990.